Available online at www.sciencedirect.com

SciVerse ScienceDirect

Journal of the European Ceramic Society 32 (2012) 1235–1244

www.elsevier.com/locate/jeurceramsoc

Low temperature sintering of $LaNbO_4$ proton conductors from freeze-dried precursors

M. Amsif [a], D. Marrero-López [b,*], J.C. Ruiz-Morales [a], S. Savvin [a], P. Núñez [a,**]

[a] *Dpto. de Química Inorgánica, Universidad de la Laguna, 38200 Tenerife, Spain*

[b] *Dpto. de Física Aplicada I, Laboratorio de Materiales y Superficies (Unidad Asociada al C.S.I.C.), Universidad de Málaga, 29071 Málaga, Spain*

Received 26 July 2011; received in revised form 9 November 2011; accepted 18 November 2011
Available online 20 December 2011

Abstract

A synthesis method based on freeze-dried precursors was used to obtain nanocrystalline powders of pure and Ca-doped $LaNbO_4$ at 800 °C. Dense ceramics were prepared at temperature as low as 1100 °C. The $LaNbO_4$ ceramics were examined by scanning electron microscopy (SEM) to study the microstructure evolution with the sintering temperature. The densification and grain growth rate are lower in Ca-doped samples. The bulk and grain boundary contributions to the overall conductivity were studied by impedance spectroscopy under different gases. Samples sintered at low temperature and with smaller grain size exhibit higher grain boundary resistance and consequently lower total conductivity.

Keywords: Proton conductor; $LaNbO_4$; Fuel cells; Precursor synthesis; Impedance spectroscopy

1. Introduction

Proton conductor oxides have been widely studied due to their potential application as electrolyte materials for fuel cells, hydrogen sensors, electrochemical hydrogen pumps, electrochemical micro-reactors, etc.[1–6]

The most studied compounds are those with perovskite-type structure (ABO_3) based on cerate or zirconates, although they show several drawbacks when operate directly with hydrocarbon fuels.[7–11] The cerates exhibit poor tolerance to carbonation due to the basicity of the alkaline-earth cation. $BaZrO_3$ based electrolytes show better chemical stability against the carbonation, but require high sintering temperatures and usually suffer from high intrinsic grain boundary resistance.

Recently, alternative proton-conducting materials have been proposed, such as those based on $LaNbO_4$ that offer high CO_2 tolerance compared to alkaline-earth containing perovskites.[12,14] This material undergoes a structural phase transition at high temperature. The low temperature phase crystallises in the monoclinic fergusonite system, whiles the high temperature phase is tetragonal with scheelite-type structure.

The conducting properties of acceptor-doped $LaNbO_4$ have been investigated in several works.[12–16] Haugrud et al. have shown that the highest ionic conductivity is found when $LaNbO_4$ is doped in the A-site with alkaline-earth cations (e.g. Ca^{2+} and Sr^{2+}).[17] The solubility limit of these cations in $LaNbO_4$ is in the range of 0.5–2 mol%. Different substitutions have been also investigated in order to suppress the fergusonite ↔ scheelite phase transformation, which may be a drawback for practical application as solid electrolyte.[18–21]

In $LaNbO_4$ the proton conductivity dominates under wet conditions up to 1000 °C with a significant p-type electronic contribution above 800 °C. The values of conductivity are one order of magnitude lower than those obtained in proton perovkites and consequently the electrolyte thickness should be reduced to the micrometric range to achieve reasonable efficiency in electrochemical devices.[22–24]

The conventional solid state reaction method, also called ceramic method, is the most used for the preparation of $LaNbO_4$. This method requires high firing temperatures to obtain single phase materials, resulting in large grain size powders. Such high sintering temperatures leave very little margin for microstructural control of the resulting ceramics and consequently temperatures of up to 1500 °C are necessary to obtain

* Corresponding author.
** Corresponding author. Tel.: +34 922318501; fax: +34 922318461.
E-mail addresses: damarre@uma.es (D. Marrero-López), pnunez@ull.es (P. Núñez).

0955-2219/$ – see front matter © 2011 Elsevier Ltd. All rights reserved.
doi:10.1016/j.jeurceramsoc.2011.11.027

dense ceramic materials. However, ceramic powders with particles in the submicrometric range are required by considering that the electrolyte thickness for $LaNbO_4$ should be in the micrometric range due to its limited ionic conductivity.

The preparative route plays also a fundamental role in the properties of the ceramic materials, controlling the microstructure, morphology and grain size, which contribute to improve the thermomechanical performance. The transport properties of the ceramic materials also depend on ceramic microstructure and specially the grain boundary contribution; because it may serve as sink for the charge carriers as well as for impurities.

Only a few synthetic methods, such as spray-pyrolysis,[26] sol–gel,[27] microwave[28] and coprecipitation[29] have been used to prepare fine powders of $LaNbO_4$. Hence, alternative synthesis routes can improve both the microstructure and conductivity of these materials. In this context, the synthesis using freeze-dried precursors has proved to be a very versatile method to synthesise a wide variety of materials.[30–33]

In this contribution Ca-doped $LaNbO_4$ have been prepared using a freeze-dried precursor route. The phase formation, densification, microstructure evolution with the temperature and conductivity under different gases have been studied.

2. Experimental

2.1. Synthesis

Polycrystalline powders of $La_{1-x}Ca_xNbO_{4-\delta}$ ($x = 0$ and 0.01) were prepared from an amorphous and dried precursor, which was obtained by freeze-drying of a solution with stoichiometric amounts of cations.

The starting reactants were: lanthanum oxide (99.99%, Aldrich), niobium ammonium oxalate (H.C. Starck 20% in Nb) and calcium nitrate (99.9% Aldrich). The lanthanum oxide was previously calcined at 1000 °C for 2 h before used to achieve dehydration and decarbonation. While the niobium ammonium oxalate was studied by thermogravimetric analysis up to 1000 °C to determine the niobium content as Nb_2O_5. The lanthanum oxide was dissolved in a diluted nitric acid solution, whereas niobium oxalate and calcium nitrate were separately dissolved in distilled water.

A solution containing ethylenediaminetetraacetic acid (EDTA) (99.5% Aldrich) and citric acid (99.5% Aldrich) in a molar ratio EDTA:citric acid:metal cations of 0.5:0.1:1 was added as complexing agent to the mixed metal solution under constant stirring. The solution pH was adjusted to 7 with the addition of concentrated ammonia, resulting in a homogeneous and transparent solution. In a typical preparation the cation concentration was adjusted to obtain approximately 5 g of oxide powders from approximately 100 ml of solution. The solutions were frozen by the dropwise addition into liquid nitrogen, retaining the cation homogeneity of the starting solution in each drop. This flash cooling process renders small ice crystals, which were dehydrated by vacuum sublimation in a Heto Lyolab 3000 freeze-drier for 2 days. In this way, dried and amorphous solid precursors were obtained. The precursor powders were immediately calcined at 300 °C to prevent rehydration and to burn out the organic material.

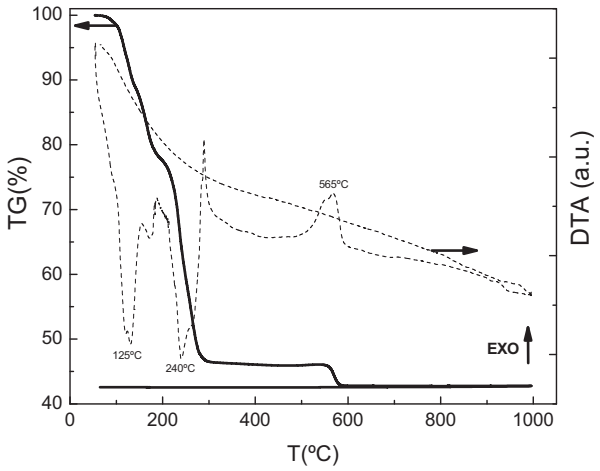

Fig. 1. TG/DTA curves of the amorphous $LaNbO_4$ precursor powders in air atmosphere.

The freeze-dried powders were investigated by TG/DTA (Perkin Elmer, Pyris Diamond) to study the thermal decomposition and the optimal crystallisation temperature of the precursors. After that the powders were calcined at 800 °C for 1 h to remove the residual organic species and to achieve crystallisation of the compounds. The polycrystalline powders were pressed into pellets and sintered between 900 and 1500 °C, for times ranging from 5 min to 4 h.

2.2. Ceramic characterisation

X-ray diffraction patterns (XRD) were recorded using a PANalytical X'Pert Pro diffractometer, equipped with a primary monochromator and the X'Celerator detector. The scans were collected in the 2θ range of 15–100° with 0.016° step for 2 h. Phase identification was performed with X'Pert HighScore Plus v.2.0a software using the JCPDS and ICSD databases for the structural models.[34]

The relative density of the sintered pellets was calculated from the mass, volume of the sample and theoretical density obtained from the structural analysis.

The morphology of the sintered pellets was examined using a scanning electron microscope (SEM) (mod. Jeol LTD, JSM-6300) combined with energy dispersive spectroscopy analysis (EDS) to detect possible phase segregations. The average grain size of the sintered pellets was estimated from the SEM micrographs, using the linear intercept method.[35]

2.3. Electrical characterisation

The as-synthesised powders at 800 °C were uniaxially pressed at 125 MPa in 1.5-mm-thick pellets with 10 mm of diameter and then sintered between 900 and 1500 °C for 5 min and 4 h. Pt-paste electrodes were applied as current collectors on each side of the pellet and then fired at 900 °C for 30 min. Impedance spectra were obtained using a frequency response

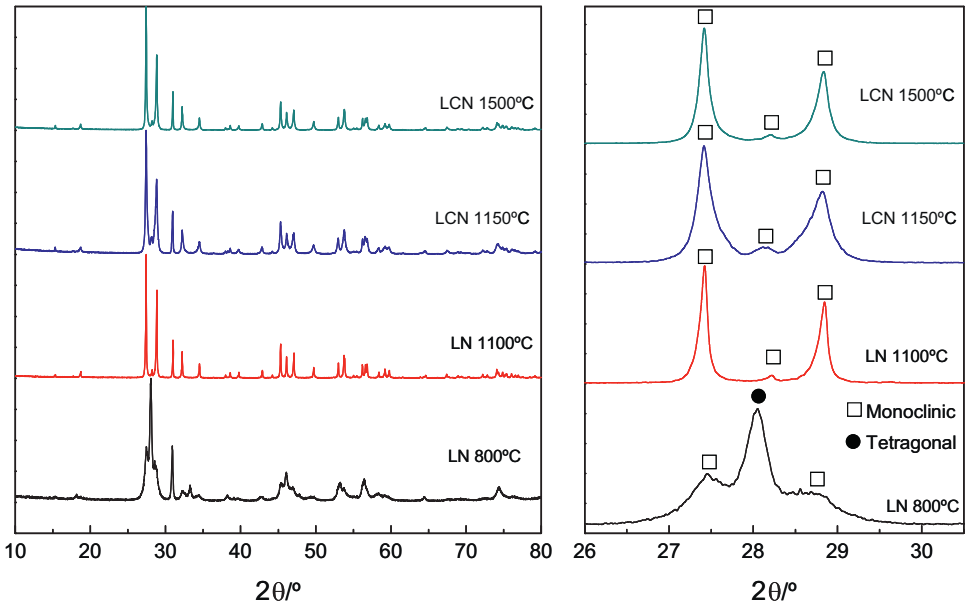

Fig. 2. XRD patterns of $LaNbO_4$ (LN) and $La_{0.99}Ca_{0.01}NbO_4$ (LCN) calcined at different temperatures between 800 and 1500 °C for 1 h.

analyser (Solartron 1260) in different dry (6 ppm H_2O) and wet (2% H_2O) gases of O_2 and 5%H_2-Ar in the 0.1 Hz to 1 MHz frequency range with an ac signal of 100 mV. The spectra were acquired during the cooling processes between 1000 and 300 °C with a dwell time of 60 min between consecutive measurements. The impedance spectra were analysed with equivalent circuits using the ZView software.[36]

3. Results and discussions

3.1. Phase formation and structure

The TGA/DTA curves of the amorphous freeze-dried precursor recorded in air show different weight loss steps between room temperature (RT) and 600 °C (Fig. 1). A first weight loss is observed from room temperature to 175 °C, which is associated to the elimination of residual water, dehydration of the precursor and removal of NO_x species. A sharp fall in the specimen weight is observed over the temperature range between 200 and 300 °C related to the oxidative decomposition of the organic material, which is an exothermic process in the DTA curve. A third decomposition step is detected around 600 °C attributed to the combustion of residual carbonaceous species. No weight losses were observed above this temperature.

The temperature evolution of XRD patterns for pure $LaNbO_4$ calcined between 800 and 1500 °C for 1 h are shown in Fig. 2. After calcined at 800 °C the ceramic powders consist in a mixture of monoclinic and tetragonal phases of $LaNbO_4$. The partial stabilisation of the tetragonal form at room temperature is mainly associated to the presence of domains as consequence of the nanocrystalline nature of the synthesised powders with an average crystallite size, estimated by the Scherrer's equation, of 45 nm for LN and 35 nm for LCN at 800 °C. However, the materials revert to the stable monoclinic phase when the firing temperature increases up to 1000 °C and the crystal size grows to 90 nm for LN and 70 nm for LCN. Above this temperature only the diffraction peaks ascribed to the monoclinic phase are observed (Fig. 2). The XRD analysis for undoped and Ca-doped $LaNbO_4$ does not show appreciable differences with the temperature. Thus Ca-substitution in $LaNbO_4$ does not contribute to retain the tetragonal form at lower temperatures. In addition Ca-doping does not shift substantially the phase transition temperature of $LaNbO_4$. This indicates that the high temperature tetragonal form is partially retained in a metastable state, when the crystallite size is below 50 nm, independently on phase composition.

3.2. Densification and microstructural characterisation

The polycrystalline powders without any previous mechanical treatment (e.g. ball milling) were pressed into pellets and sintered between 900 and 1500 °C for 4 h to study the densification and grain growth behaviour (Fig. 3).

The relative density of undoped $LaNbO_4$ (LN) increases with the sintering temperature from 55% at 900 °C to nearly fully dense at 1100 °C. The incorporation of 1 mol% of Ca in $LaNbO_4$ (LCN) increases the temperature necessary to obtain dense ceramics with relative density of 58% at 1000 °C and 99% at 1150 °C. This shift to higher temperatures in Ca-doped $LaNbO_4$ indicates that the dopants reduce the densification rate. Considering that densification is usually controlled by grain boundary diffusion, this result confirms that the dopant cations modify the structure of the grain boundary region of undoped $LaNbO_4$.

It should be commented that this sintering temperature is lower than that of the traditional method by solid state reaction 1500 °C, and even somewhat lower than that reported previously by spray-pyrolysis 1200 °C.[25] This low sintering temperature is useful to avoid excessive grain growth. The microstructural features (e.g. grain size) may be adjusted by extending the

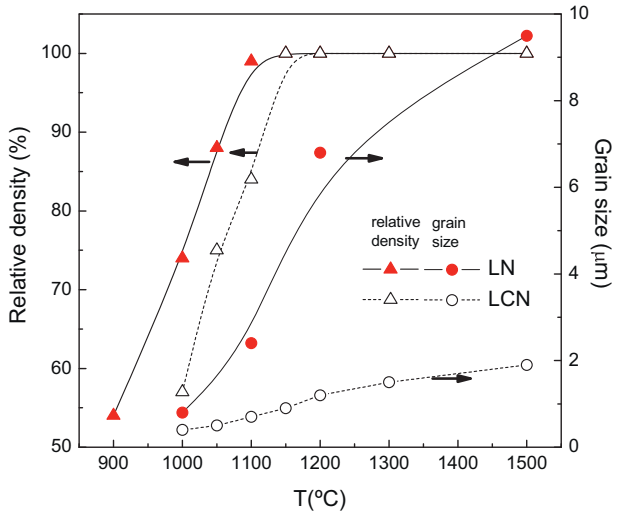

Fig. 3. Evolution of relative density and grain size for $LaNbO_4$ (LN) and $La_{0.99}Ca_{0.01}NbO_{4-\delta}$ (LCN) ceramics sintered at different temperatures for 4 h.

sintering time and/or temperature and to optimise the corresponding grain boundary effects on transport properties and/or thermomechanical performance. In addition, this temperature range is sufficiently low to allow the co-sintering between the electrolyte and electrode materials, preventing excessive interdiffusion/reactivity between the different layers of the cell.

The temperature evolution of the ceramic microstructure for undoped and Ca-doped $LaNbO_4$ is shown in Fig. 4. As can be observed, the ceramics exhibit negligible porosity above 1000 and 1100 °C for LN and LCN samples, respectively. Phase segregations were not detected in any of the samples investigated. It is also observed that the grain size is smaller in Ca-doping samples. On the other hand, pellets of undoped $LaNbO_4$ show microcracks after sintering above 1200 °C and the number of microcracks increases with the sintering temperature (Fig. 4d) and sintering time (Fig. 5c). This is possibly related to the grain growth with increasing temperature and time. No microcracks were observed in samples with Ca-doping (Fig. 4e–h) and (Fig. 5d–f). It has been reported that the grain size has a significant influence on mechanical properties of $LaNbO_4$ materials. Indeed, values of fracture strength as low as 35 MPa have been reported,[37] which is possibly attributed to microcracks formation above a critical grain size as a consequence of the anisotropic thermal expansion. This also explains the variation in Vickers hardness with values ranging between 3 and 6 GPa for samples with grain size of 12 and 2 μm, respectively.[26] These results confirm the importance of controlling the grain size during the sintering of $LaNbO_4$ based materials.

The SEM micrographs were analysed to evaluate the corresponding average grain size with the temperature. The average grain size of pure $LaNbO_4$ increases with the temperature from 0.8 μm at 1000 °C to 9.5 μm at 1500 °C, whereas 1% Ca doped $LaNbO_4$ shows smaller variation in the grain size from 0.4 μm at 1000 °C to 1.9 μm at 1500 °C (Fig. 3).

The influence of time on the densification processes was also evaluated. In both undoped and Ca-doped samples, the densification takes place in a short interval of time (Fig. 5). Dense pellets with relative density higher than 95% were obtained for all the samples after sintering at 1150 °C for only 30 min. In addition, at a fixed temperature the grain size grows with the sintering time and the increase is most significant for undoped samples (Fig. 5).

The low densification temperature of lanthanum niobate ceramics, obtained by freeze-drying, allows studying the grain growth behaviour in a wide range of temperatures. The evolution of the microstructure and the grain growth in ceramic materials can be analysed using the growth kinetics equation.[38]

$$D^n - D_o^n = K_o \cdot t \cdot e^{-Q/RT} \quad (1)$$

where D is the average grain size with the time t, D_o is the initial grain size of the polycrystalline powders at time ($t = 0$), K_o is a rate constant, Q is the activation energy of grain growth and n is an exponent, which is an integer ranging from 2 to 4 depending upon various kinetic aspects involved in the growth process.[38]

The grain size of the starting ceramic powders D_o is smaller than D and consequently the term D_o^n can be neglected in comparison to D^n. Therefore, Eq. (1) can be simplified as follows:

$$\frac{D^n}{t} = K_o e^{-Q/RT} \quad (2)$$

and in logarithmic scale:

$$\ln\left(\frac{D^n}{t}\right) = \ln K_o - \frac{Q}{RT} \quad (3)$$

In a suitable temperature range the activation energy Q is constant and thus the exponent n can be determined from the slope in the plot of $\ln(D)$ versus $\ln(t)$ (Fig. 6a). In consequence, the activation energy Q can be obtained from the slope of the Arrhenius plot of $\ln(D^n/t)$ versus $1/T$ (Fig. 6b). The growth exponent n takes a value around 4 for samples with and without Ca-doping, suggesting that densification rate is controlled by grain boundary diffusion.

The activation energy for grain growth in the temperature range 1000–1200 °C depends significantly of Ca-doping with a value of 700 kJ/mol for undoped $LaNbO_4$ and 420 kJ/mol for $La_{0.99}Ca_{0.01}NbO_{4-\delta}$. The activation energies for grain growth of lanthanum niobates have not been reported previously to compare with the literature, however similar values have been given for other solid electrolytes (i.e. 697 kJ/mol for Gd-doped CeO_2[39] and 650 kJ/mol for $La_{0.8}Sr_{0.2}Ga_{0.8}Mg_{0.2}O_{3-\delta}$[33]).

The densification and grain growth behaviour in ceramic materials are influenced by several factors, such as morphology of the starting powders, doping segregations at the grain boundary, defect interaction and lattice distortion induced by the doping. In addition, the inhibition of the grain growth is usually associated to a reduction of grain boundary mobility and energy by impurities, pores or particles of a secondary phase.

In the present study the powders of $LaNbO_4$ and $La_{0.99}Ca_{0.01}NbO_{4-\delta}$ were prepared following the same procedure and exhibit similar grain size with low aggregates; hence different densification process due to powder morphology is considered negligible. Hence, the differences in grain growth in undoped and Ca-doped $LaNbO_4$ can be related to segregation of the dopant cations at the grain boundaries, which lowers grain

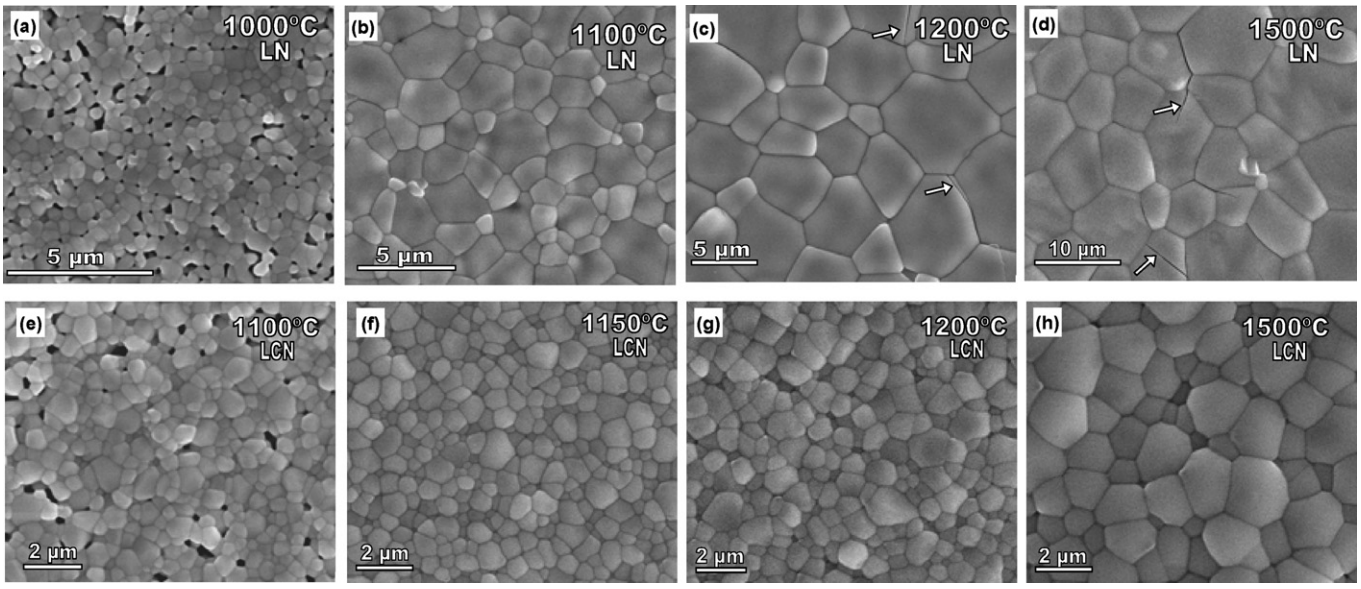

Fig. 4. SEM images of surface pellets of (a–d) $LaNbO_4$ (LN) and (e–h) $La_{0.99}Ca_{0.01}NbO_{4-\delta}$ (LCN) sintered between 1000 and 1500 °C for 4 h. Microcracks for LN are indicated by arrows (c and d).

boundary mobility and grain boundary energy, thus increasing the cohesive strength of the grain boundary and the diffusion distance across the boundary.

The inhibition effects of dopant on grain growth have previously been observed in many other ceramic materials, such as doped CeO_2,[40] and doped ZrO_2[41] and were usually described on the basis of the space charge model. This model considers that the excess of dopant at the grain boundary generates a concentration gradient between the grain interior and grain boundary regions that retains the diffusion of cations and consequently the densification and grain growth rate decrease.

Considering that Ca-doping reduces the cation mobility and grain growth, one would expect larger activation energy for grain growth in Ca-doped samples, contrary to the obtained results. A significant variation in the interfacial energy at the grain boundary could explain this anomalous behaviour. On the other hand, the variation of grain size for $La_{0.99}Ca_{0.01}NbO_{4-\delta}$ is very small with both temperature and time; varying between

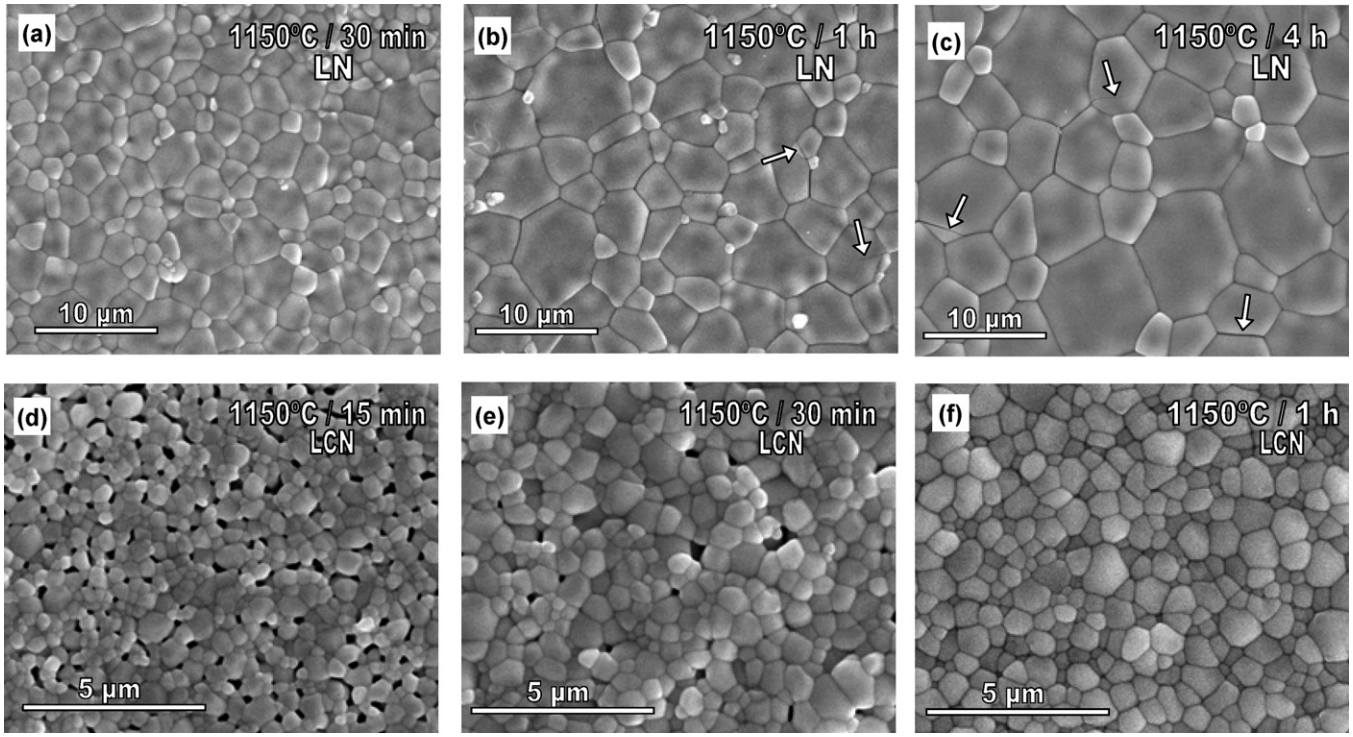

Fig. 5. SEM images of surface pellets of (a–c) $LaNbO_4$ (LN) and (d–f) $La_{0.99}Ca_{0.01}NbO_{4-\delta}$ (LCN) sintered at 1150 °C for different times. Microcracks for LN are indicated by arrows (b and c).

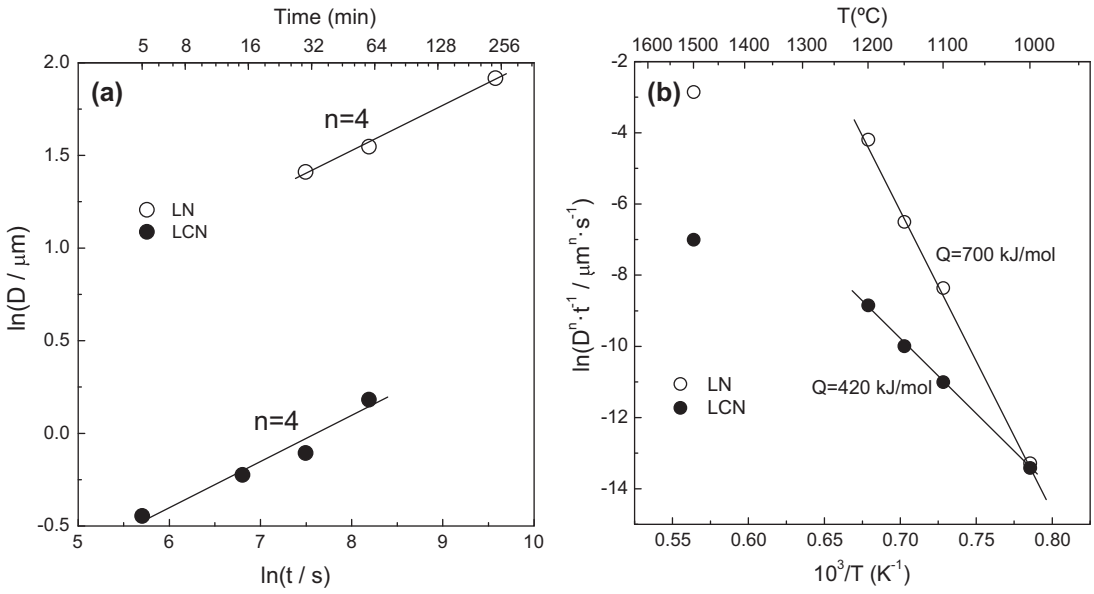

Fig. 6. (a) Temporal and (b) temperature evolution of grain size for $LaNbO_4$ (LN) and $La_{0.99}Ca_{0.01}NbO_{4-\delta}$ (LCN) samples sintered at different temperatures.

0.6 and 1.2 μm at 1150 °C for sintering times between 5 and 60 min, respectively, and remaining almost constant for longer sintering time. Hence, the error in the determination of the grain growth exponent is high and consequently the activation energy for grain growth could be different from that obtained for $La_{0.99}Ca_{0.01}NbO_{4-\delta}$. Samples with lower Ca-doping should be studied to further understand the effects of calcium on the grain growth kinetics of $LaNbO_4$.

3.3. Electrical characterisation

The impedance spectra in the low temperature range for $La_{0.99}Ca_{0.01}NbO_4$ (LCN) samples sintered at 1150 and 1500 °C for 4 h comprise three separated contributions (Fig. 7). The spectra were analysed with equivalent circuits formed by (*RQ*) elements in series, where *R* is a resistance and *Q* a pseudo-capacitance in parallel; thus the following equivalent circuit

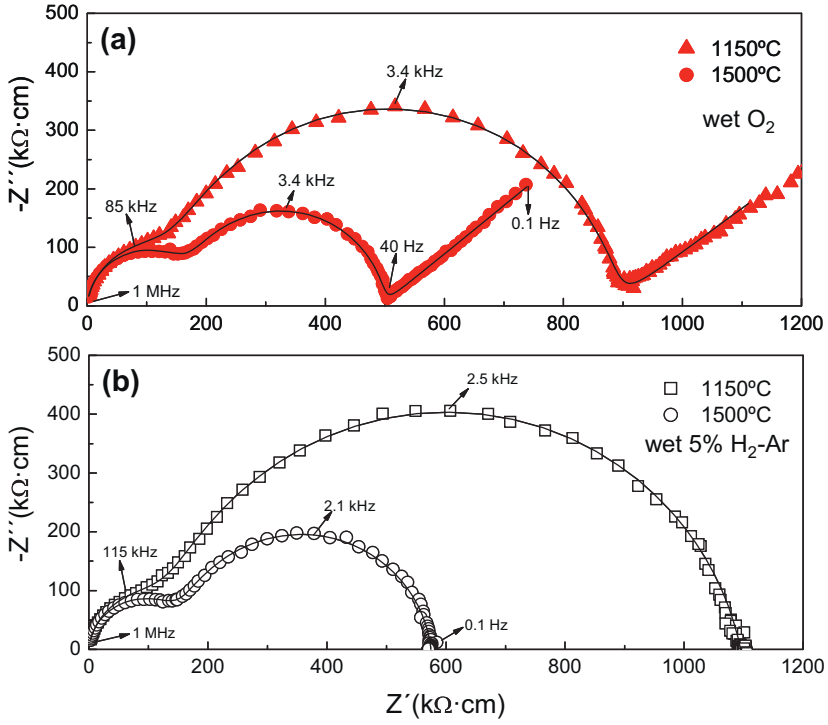

Fig. 7. Impedance spectra at 400 °C for $La_{0.99}Ca_{0.01}NbO_{4-\delta}$ pellets sintered at 1150 and 1500 °C for 4 h under (a) wet O_2 and (b) wet 5%H_2-Ar. The solid line represents the fitting curves obtained with equivalent circuits.

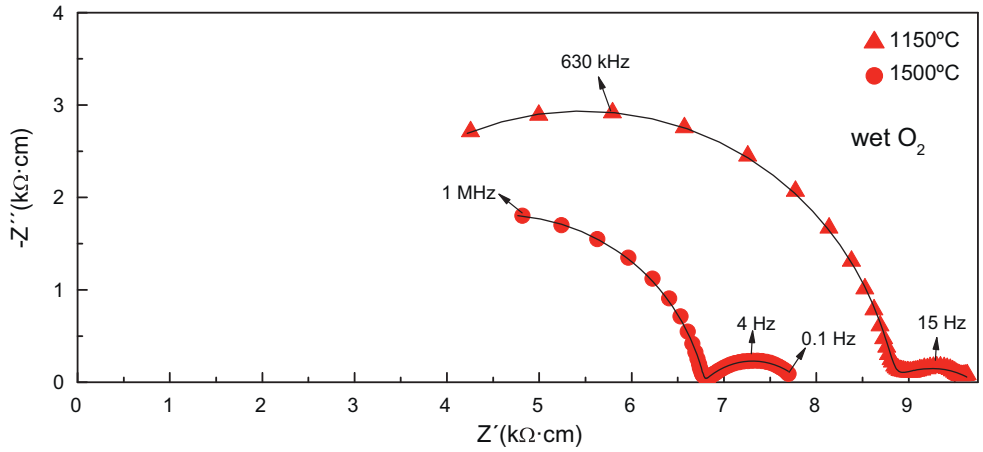

Fig. 8. Impedance spectra at 700 °C for $La_{0.99}Ca_{0.01}NbO_{4-\delta}$ pellets sintered at 1150 and 1500 °C for 4 h under wet O_2. The solid line represents the fitting curves obtained with equivalent circuits.

$(R_1Q_1)(R_2Q_2)(Q_3)$ was used to fit the data. The capacitance values of the different processes are about 5 pF cm^{-1}, 10 nF cm^{-1} and 10 μF cm^{-1} for the high, intermediate and low frequency contributions and therefore they can be ascribed to grain interior, grain boundary and electrode processes, respectively.

The impedance spectra for undoped $LaNbO_4$ show only a broad semicircle with capacitance of 10 pF cm^{-1}, which can be ascribed to bulk contribution. The grain boundary resistance in this sample seems to be negligible compared to bulk one.

The grain boundary in Ca-doped $LaNbO_4$ is the main resistive contribution of the electrolyte in the low temperature range in both wet O_2 (Fig. 7a) and wet 5%H_2-Ar gases (Fig. 7b). The bulk is practically independent of the sintering temperature; while the grain boundary contribution is larger in those samples prepared at lower temperature due to the smaller grain size and consequently the increase of the number of grain boundaries across the sample.

In the high temperature range (Fig. 8) the electrode contributions are dominant because the relaxation frequency of the electrolyte responses are shifted to higher frequencies and only the total conductivity of the electrolyte can be determined. In this case, the equivalent circuit used to fit the spectra is denoted as: $R_s(R_1Q_1)(R_2Q_2)$, where R_s is a serial resistance ascribed to the bulk contribution of the electrolyte and the high and low frequency arcs are associated to the grain boundary and electrodes processes with capacitance values of 5 nF cm^{-1} and 10 mF cm^{-1}, respectively.

The grain interior (R_b) and grain boundary resistances (R_{gb}) were used to obtain the bulk and macroscopic grain boundary conductivities, taking into account the sample geometry:

$$\sigma_i = \frac{L}{R_i S} \tag{4}$$

where L is the sample thickness and S is the electrode area of the pellets. The values of conductivity were plotted using the Arrhenius equation:

$$\sigma = \frac{\sigma_0}{T} \exp\left(-\frac{E_a}{kT}\right) \tag{5}$$

The temperature dependence of the grain interior conductivity is shown in Fig. 9. As can be observed, the bulk conductivity for LCN samples is almost one order of magnitude lower in dry Ar than in wet O_2 and 5%H_2-Ar, indicating a predominant proton contribution in wet atmosphere. It should be also noted that the bulk conductivity is practically the same for samples sintered at 1150 and 1500 °C. The bulk conductivity for undoped $LaNbO_4$, without oxygen vacancies in the structure, is three orders of magnitude lower than that of Ca-doped samples.On the other hand the macroscopic grain boundary conductivity decreases with increasing the sintering temperature (Fig. 10a). This trend, as previously commented, is related to the different grain sizes with the sintering temperature. Indeed, very similar conductivity values are found when the grain boundary resistance is normalised by the grain size to take into account differences in the number of grain boundaries across the sample (Fig. 10b). In addition, the macroscopic grain boundary conductivity is very

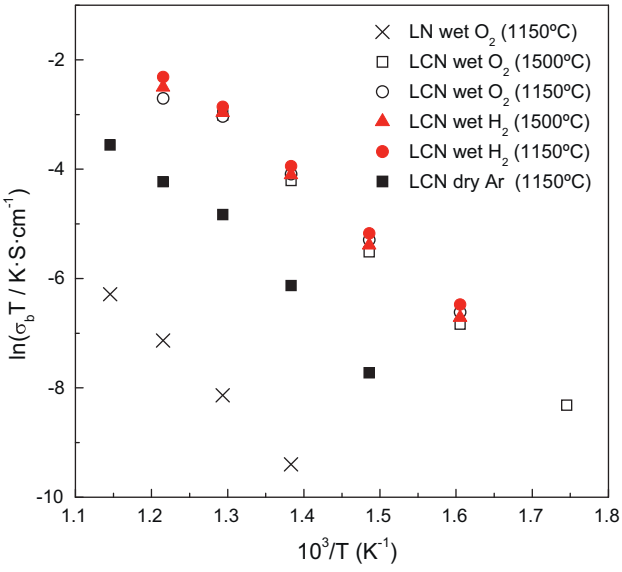

Fig. 9. Arrhenius plots of the bulk conductivity, under different dry/wet gases, for $La_{0.99}Ca_{0.01}NbO_{4-\delta}$ pellets sintered at 1150 and 1500 °C for 4 h and undoped $LaNbO_4$ (LN) pellet sintered at 1150 °C.

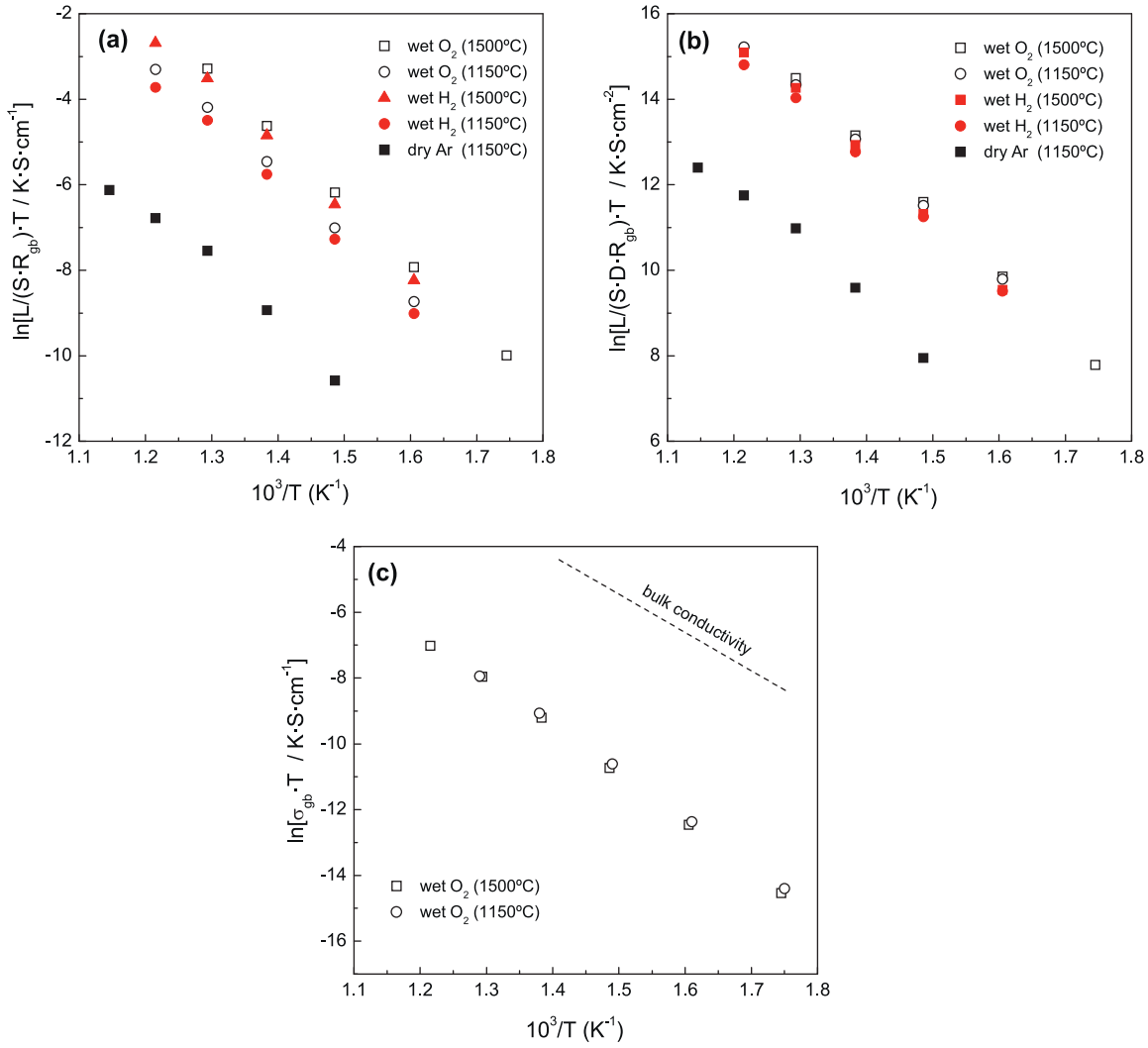

Fig. 10. Arrhenius plots of the (a) macroscopic grain boundary conductivity, (b) macroscopic grain boundary conductivity after normalisation by the ceramic grain size and (c) specific grain boundary conductivity for $La_{0.99}Ca_{0.01}NbO_{4-\delta}$ pellets sintered at 1150 and 1500 °C for 4 h.

similar in wet O_2 and 5%H_2-Ar atmospheres but lower in dry gases, following the same trend as the bulk contribution.

The specific grain boundary conductivity σ_{gb} was estimated under the assumption that the dielectric constant of the grain boundary is very close to that of the bulk ($\varepsilon_{gb} \approx \varepsilon_b = 19$[16]).

$$\sigma_{gb} = \frac{\varepsilon_o \varepsilon_{gb}}{C_{gb} R_{gb}} = w_{gb} \varepsilon_o \varepsilon_{gb} \quad (6)$$

The values σ_{gb} are two orders of magnitude lower than those of the bulk (Fig. 10c). In addition, the sintering temperature has not influence on the grain boundary specific conductivity.

The Arrhenius plots of the overall conductivity under different atmospheres are shown in Fig. 11. The curves present a change in the slope around 500 °C that coincides with the monoclinic to tetragonal phase transformation. One can observe that the lowest conductivity values are found in dry Ar in the whole temperature range studied. An enhancement of the conductivity of about one order of magnitude is observed in wet atmospheres of 5%H_2-Ar and O_2 due to the presence of a significant proton contribution. In the high temperature range, the conductivity under wet O_2 is higher than under 5%H_2-Ar, evidencing a significant p-type contribution.

The values of conductivity are slightly larger for samples sintered at 1500 °C than at 1150 °C (e.g. 8×10^{-4} and 6×10^{-4} S cm^{-1} for samples prepared at 1500 and 1150 °C, respectively, at 950 °C under wet O_2) and it could be ascribed to the different grain boundary contributions of the samples to the overall conductivity. However, these values of conductivity are similar to those reported previously, i.e. 10^{-3} S cm^{-1}.[13]

In summary, the freeze drying is an useful method to obtain polycrystalline powders of $LaNbO_4$-based materials at low temperature as 1000 °C. Dense ceramics with relative density higher than 98% were obtained after sintering between 1100 and 1150 °C. This low sintering temperature avoids an excessive grain growth and the formation of fractures during the sintering process. The densification and grain growth of $LaNbO_4$ are retained after calcium doping.

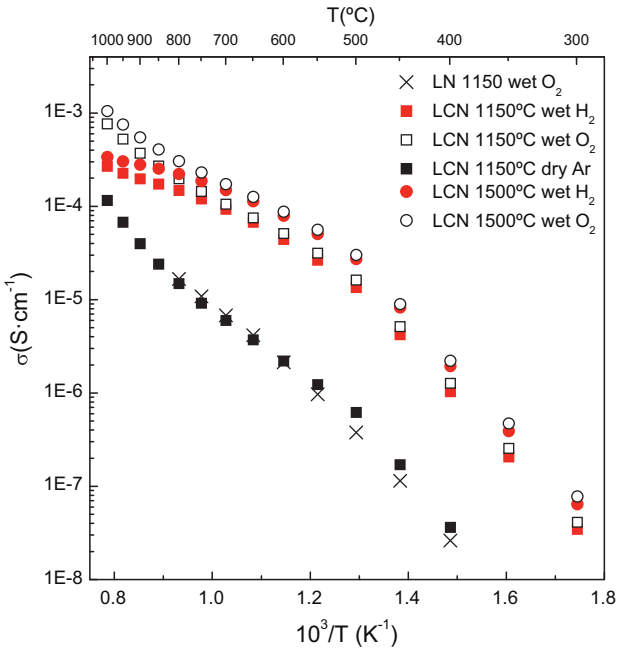

Fig. 11. Arrhenius representation of the overall conductivity for $La_{0.99}Ca_{0.01}NbO_{4-\delta}$ (LCN) and undoped $LaNbO_4$ (LN) pellets sintered at 1150 and 1500 °C for 4 h.

In the samples prepared at low temperature, the grain boundary is the main contribution to the overall conductivity, however the values of conductivity obtained in the high temperature range 8×10^{-4} S cm^{-1} at 950 °C under wet O_2 are comparable to those previously reported.

Acknowledgements

This work was supported by the Spanish Research Program (MAT2010-16007) and Canary Islands Government (PI2007/020).

References

1. Norby T. Solid-state protonic conductors: principles, properties, progress and prospects. *Solid State Ionics* 1999;**125**:1–11.
2. Orera A, Slater PR. New chemical systems for solid oxide fuel cells. *Chem Mater* 2010;**22**:675–90.
3. Malavasi L, Fisher CAJ, Islam MS. Oxide-ion and proton conducting electrolyte materials for clean energy applications: structural and mechanistic features. *Chem Soc Rev* 2010;**39**:4370–87.
4. Phair JW, Badwal SPS. Review of proton conductors for hydrogen separation. *Ionics* 2006;**12**:103–15.
5. Kreuer KD. Proton-conducting oxides. *Annu Rev Res* 2003;**33**:333–59.
6. Schober T. Applications of oxidic high-temperature proton conductors. *Solid State Ionics* 2003;**162–163**:277–81.
7. Bonanos N. Transport properties and conduction mechanism in high-temperature protonic conductors. *Solid State Ionics* 1992;**53–56**:967–74.
8. Norby T. Proton conductivity in perovskite oxides. In: Ishihara T, editor. *Perovskite oxide for solid oxide fuel cells*. Springer; 2009. p. 217–41.
9. Bonanos N, Knight KS, Ellis B. Perovskite solid electrolytes: structure, transport properties and fuel cell applications. *Solid State Ionics* 1995;**79**:161–70.
10. Iwahara H, Uchida H, Ono K, Ogaki K. Proton conduction in sintered oxides based on $BaCeO_3$. *J Electrochem Soc* 1988;**135**:529–33.
11. Ryu KH, Haile SM. Chemical stability and proton conductivity of doped $BaCeO_3$–$BaZrO_3$ solid solutions. *Solid State Ionics* 1999;**125**:355–67.
12. Haugsrud R, Norby T. Proton conduction in rare earth ortho-niobates and orthotantalates. *Nat Mater* 2006;**5**:193–6.
13. Haugsrud R, Norby T. High-temperature proton conductivity in acceptor-doped $LaNbO_4$. *Solid State Ionics* 2006;**177**:1129–35.
14. Magrasó A, Fontaine ML, Larring Y, Bredesen R, Syvertsen GE, Lein HL, et al. Development of proton conducting SOFCs based on $LaNbO_4$ electrolyte – status in Norway. *Fuel Cells* 2011;**11**:17–25.
15. Fjeld H, Toyoura K, Haugsrud R, Norby T. Proton mobility through a second order phase transition: theoretical and experimental study of $LaNbO_4$. *Phys Chem Chem Phys* 2010;**12**:10313–9.
16. Fjeld H, Kepaptsoglou DM, Haugsrud R, Norby T. Charge carriers in grain boundaries of 0.5% Sr-doped $LaNbO_4$. *Solid State Ionics* 2010;**181**:104–9.
17. Mokkelbost T, Kaus I, Haugsrud R, Norby T, Grande T, Einarsrud MA. High-temperature proton-conducting lanthanum ortho-niobate-based materials. Part II: sintering properties and solubility of alkaline earth oxides. *J Am Ceram Soc* 2008;**91**:879–86.
18. Brandão AD, Antunes I, Frade JR, Torre J, Kharton VV, Fagg DP. Enhanced low-temperature proton conduction in $Sr_{0.02}La_{0.98}NbO_{4-\delta}$ by scheelite phase retention. *Chem Mater* 2010;**22**:6673–83.
19. Mather GC, Fisher CAJ, Islam MS. Defects, dopants, and protons in $LaNbO_4$. *Chem Mater* 2010;**22**:5912–7.
20. Solís C, Serra JM. Adjusting the conduction properties of $La_{0.995}Ca_{0.005}NbO_{4-\delta}$ by doping for proton conducting fuel cells electrode operation. *Solid State Ionics* 2011;**190**:38–45.
21. Brandão AD, Gracio J, Mather GC, Kharton VV, Fagg DP. B-site substitutions in $LaNb_{1-x}M_xO_{4-\delta}$ materials in the search for potential proton conductors (M = Ga, Ge, Si, B, Ti, Zr, P, Al). *J Solid State Chem* 2011;**184**:863–70.
22. Fontaine ML, Larring Y, Haugsrud R, Norby T, Wiik K, Bredesen R. Novel high temperature proton conducting fuel cells: production of $La_{0.995}Sr_{0.005}NbO_{4-\delta}$ electrolyte thin films and compatible cathode architectures. *J Power Sources* 2009;**188**:106–13.
23. Magrasó A, Haugsrud R, Norby T. Preparation and characterization of Ni–$LaNbO_4$ cermet anode supports for proton-conducting fuel cell applications. *J Am Ceram Soc* 2010;**93**:2650–5.
24. Lin B, Wang S, Liu X, Meng G. Stable proton-conducting Ca-doped $LaNbO_4$ thin electrolyte-based protonic ceramic membrane fuel cells by in situ screen printing. *J Alloys Compd* 2009;**478**:355–7.
25. Mokkelbost T, Andersen Ø, Strøm RA, Wiik K, Grande T, Einarsrud MA. High-temperature proton-conducting $LaNbO_4$-based materials: powder synthesis by spray pyrolysis. *J Am Ceram Soc* 2007;**90**:3395–400.
26. Mokkelbost T, Lein HL, Vullum PE, Holmestad R, Grande T, Einarsrud MA. Thermal and mechanical properties of $LaNbO_4$-based ceramics. *Ceram Int* 2009;**35**:2877–83.
27. Hsiao YJ, Fang TH, Chang YS, Chang YH, Liu CH, Ji LW, et al. Structure and luminescent properties of $LaNbO_4$ synthesized by sol–gel process. *J Lumin* 2007;**126**:866–70.
28. Lee HW, Park JH, Nahm S, Kim DW, Park JG. Low-temperature sintering of temperature-stable $LaNbO_4$ microwave dielectric ceramics. *Mater Res Bull* 2010;**45**:21–4.
29. Gupta UN, Pradhan S, Muthurajan H, Kumar HH, Kharat DK, Ravi V. A co-precipitation technique of preparing $LaNbO_4$ powders. *J Am Ceram Soc* 2007;**90**:2661–3.
30. Marrero-López D, Peña-Martínez J, Pérez-Coll D, Núñez P. Effects of preparation method on the microstructure and transport properties of $La_2Mo_2O_9$ based materials. *J Alloys Compd* 2006;**422**:249–57.
31. El-Himri A, Marrero-López D, Núñez P. Pt_2Mo_3N and $PdPtMo_3N$: new interstitial nitrides prepared from freeze-dried precursors. *J Solid State Chem* 2004;**177**:3219–23.
32. Amsif M, Marrero-López D, Magrasó A, Peña-Martínez J, Ruiz-Morales JC, Núñez P. Synthesis and characterisation of $BaCeO_3$-based proton conductors obtained from freeze-dried precursors. *J Eur Ceram Soc* 2009;**29**:131–8.
33. Marrero-López D, Martín-Sedeño MC, Peña-Martínez J, Ruiz-Morales JC, Núñez P, Ramos-Barrado J.R. Microstructure and conductivity of

$La_{1-x}Sr_xGa_{0.8}Mg_{0.2}O_{3-\delta}$ electrolytes prepared using the freeze-drying method. *J Am Ceram Soc* 2011;**94**:1031–9.
34. *X'Pert HighScore Plus, version 2.2d*. PANalytical BV; 2004.
35. Abrantes JCC. *Estereologia, software package*. Portugal: ESTG/IPVC; 2001.
36. Johnson D. *ZView: a software program for IES analysis, version 2.8*. Southern Pines. NC: Scribner Associates, Inc.; 2002.
37. Takagi T, Choa YH, Sekino T, Niihara K. Fabrication and mechanical properties of $LaNbO_4$ and $LaNbO_4/Al_2O_3$. *Key Eng Mater* 1999;**161**(163):181–4.
38. Dutta SK, Sprigge RM. Grain growth in fully dense ZnO. *J Am Ceram Soc* 1970;**53**:61–2.
39. Zhang T, Hing P, Huang H, Kilner JA. Sintering and grain growth of CoO-doped CeO_2 ceramics. *J Eur Ceram Soc* 2002;**22**:27–34.
40. Li JG, Ikegami T, Mori T. Low temperature processing of dense samarium-doped CeO_2 ceramics: sintering and grain growth behaviors. *Acta Mater* 2004;**52**:2221–8.
41. Guo X, Waser R. Electrical properties of the grain boundaries of oxygen ion conductors: acceptor-doped zirconia and ceria. *Prog Mater Sci* 2006;**51**:151.